Infrared Spectrum of *p*-Benzoquinone in Water Obtained from a QM/MM Hybrid Molecular Dynamics Simulation

Marco Nonella, Gerald Mathias, and Paul Tavan*

Theoretische Biophysik, Lehrstuhl für BioMolekulare Optik, Ludwig-Maximilians-Universität München, Oettingenstrasse 67, D-80538 München, Germany

Received: December 17, 2002; In Final Form: July 15, 2003

The accurate description of vibrational spectra of isolated dye molecules such as quinones has become a standard task in computational chemistry due to the progress of density functional theory. This is by no means the case for solution spectra. To contribute to this issue, we have carried out a QM/MM hybrid molecular dynamics (MD) simulation of *p*-benzoquinone in water, so as to derive its IR spectra. We have explored two different computational procedures that allow the calculation of an IR spectrum from such a dynamics simulation. One is based on Fourier transforms of autocorrelation functions and the other on instantaneous normal-mode analyses of snapshots. We show that both approaches are valid and yield similar vibrational frequencies. For a detailed comparison of computed bandwidths and intensities, however, our 17.5 ps QM/MM-MD trajectory turned out to be too short. The analysis of the trajectory also demonstrates that, on the average, three water molecules form distinct solvation shells around each of the quinone C═O groups. These hydrogen bonded water molecules exchange on a time scale of about 2.5 ps. Computations on small, rigid quinone-water clusters compare reasonably well with the dynamics approach concerning the spectral positions of the quinone IR bands. Of course, the inhomogeneous broadening of IR bands, which is covered by the dynamics calculations, is inaccessible to the static cluster approach.

1. Introduction

The intramolecular force fields of dye molecules are strongly affected by solvation. In polar solvents, like water, or in complex solvents, like proteins, these solvation effects are witnessed by distinct and sizable band shifts in the IR spectra of the solute dye molecules. An important class of biological dyes is formed by the quinones, which actively take part in the redox reactions of respiration and photosynthesis.[1]

As a specific example, consider the bacterial photosynthetic reaction center of *Rb. sphaeroides*. This protein has two chemically identical quinones carrying out two different functions. After light-induced charge separation at the so-called "special pair" of bacteriochlorophyll molecules, the primary quinone Q_A accepts an electron and transfers it to the secondary quinone Q_B. These redox reactions represent essential steps in the photosynthetic light-energy conversion.[2] They can be monitored by time-resolved FTIR difference spectroscopy,[3−5] because the spectral locations of the prominent C═O and C═C stretching bands drastically differ in Q_A and Q_B, respectively, and experience large changes during electron transfer. It has been a challenge for computational chemistry to provide a microscopic explanation for these differences in terms of specific interactions of the two quinones with their respective protein surroundings.

Recently, this task has been tackled by Nonella et al.[6] by applying a highly accurate quantum mechanical (QM) description to the quinone dyes and a sufficiently accurate molecular mechanics (MM) treatment to the protein environment using a hybrid QM/MM Hamiltonian.[7] The particular QM/MM hybrid method applied here has been specifically designed for the computation of vibrational spectra in condensed phase.[8] Therefore, it combines density functional theory (DFT), which is known to yield highly accurate force fields for polyatomic molecules isolated in the vacuum,[9,10] with an MM approach properly accounting for the long-range electrostatic interactions in large solvent systems.[11] The viability of this QM/MM method for the computation of vibrational spectra had been established by detailed investigations of the water dimer and of a QM water molecule dissolved in bulk MM water.[8]

In the work of Nonella et al.,[6] a rather simple minded approach has been chosen for the QM/MM computation of the IR spectra of Q_A and Q_B in *Rb. sphaeroides*: First, the coordinates of this protein were taken from two different X-ray crystal structures.[12,13] Subsequently, the QM/MM force field was used for the energy minimization of these protein structures. Finally, the Hessians were calculated for the QM-fragments in their rigid protein cages yielding quinone line spectra. Within the classification scheme of Cui and Karplus,[14] this procedure corresponds to a complete neglect of the kinetic couplings between the QM- and MM-fragments in the computation of the IR spectra. As shown by the same authors,[14] this approximation has negligible effects on calculated frequencies and changes intensities only a little. As a result, Nonella et al. were able to reproduce the observed IR spectra of Q_A with an accuracy of a few wavenumbers, to explain the unusually low frequency of one of its C═O stretching modes by specific electrostatic interactions with the iron cofactor of the protein and to infer from differences between observed and calculated IR spectra of Q_B that the X-ray structures[12,13] are erroneous near the binding pocket of Q_B.

However, these conclusions partially rely on the assumption that the applied QM/MM method can generally describe condensed-phase IR spectra at an accuracy comparable to the

* To whom correcpondence should be addressed. E-mail: tavan@physik.uni-muenchen.de.

10.1021/jp027747r CCC: $25.00
Published on Web 09/18/2003

one that now is standard in gas-phase descriptions.[10] To validate this assumption, applications of this QM/MM technique to molecules in homogeneous solutions are required, because here all those difficulties are absent, which are connected with the complex structures of protein environments and with the experimental problems of accurately determining these structures. Furthermore, it is experimentally much easier to measure the IR spectra of molecules in solution than in proteins. The absence of the protein-specific difficulties addressed above does not imply, however, that the computation of the IR spectra of molecules in homogeneous solutions is an easy task. On the contrary, for this purpose, suitable methods, which, in addition to band frequencies, also provide inhomogeneously broadened bandwidths, are yet to be established.

In this paper, we therefore want to explore two alternative protocols by which one can determine IR spectra of solute molecules within the QM/MM framework. One of these protocols, is based on Fourier transforms of time-correlation functions (FTTCF) derived from a QM/MM molecular dynamics (MD) trajectory and the other on instantaneous normal-mode analyses (INMA) of the solute in a set of statistically independent solvent cages taken from this trajectory. Whereas the former protocol appears to be natural for the computation of vibrational spectra from MD simulations, the latter requires explanations:

(a) In the usual experimental approach, the mode compositions of the bands observed in vibrational spectra are characterized by considering a series of isotope substitutions. Thus, for theoretical descriptions, one should have access to Hessian matrixes, from which all isotope effects can be derived at a negligible computational effort. Furthermore, the Hessians yield normal modes, which allow straightforward analyses of mode compositions. In contrast, within the FTTCF approach, the analysis of each isotope substitution requires the computation of a separate QM/MM MD trajectory, which is computationally most expensive.

(b) At room temperature, the solvent shell, which surrounds a solute molecule, constantly fluctuates, assuming a variety of different conformations. In a given conformation, the solvent cage generates a specific electrostatic field within the volume occupied by the solute and thus specifically modifies its intramolecular force field by polarization of its electron distribution. In view of the concepts[15] underlying the Born−Oppenheimer approximation, one can safely assume that this electrostatic polarization is the key cause for the observed solvent shifts of the vibrational bands. Correspondingly, the variations of this polarization, which are associated with the fluctuations of the solvent cage, can be assumed to cause the inhomogeneous broadenings. These assumptions have to be computationally verified, of course: During an MD simulation, various solvent shell conformations are sampled. This sampling will cover all relevant and statistically independent solvent shell conformations if the MD trajectory extends over many multiples of the dielectric relaxation time of the solvent (assuming that the solvent fluctuates about as rapidly near the surface of the solute as in the bulk). In the case of water, the relaxation time is in the range of a few picoseconds. Thus, for sufficient statistics, an MD trajectory of a solute in aqueous solution should cover at least a few tens of picoseconds.

(c) By selecting snapshots from an MD trajectory at time lags of a few picoseconds, one can hope to obtain a set of solvent cage structures, which represent a prototypical set of conformations. Now the question arises of how one should determine the minimum energy configurations required for the computation of Hessians from the snapshots. For instance, if one takes the snapshot structures as starting points for a joint minimization of the QM/MM Hamiltonian of the whole solvent−solute system, as suggested by Cui and Karplus,[14] one obtains other structures corresponding to the nearest minima of the potential energy surface in configuration space. Whether the solvent cages in these structures are still suitable representatives of the room temperature solvent shell conformations is unknown. Therefore, we suggest keeping the instantaneous structures of the solvent at the snapshots fixed and adjusting only the solute molecule to these rigid cages by energy minimization. As compared to the proposal of Cui and Karplus,[14] this protocol saves a huge amount of computation time, because the minimization becomes restricted to the few degrees of freedom of the solute, entailing a rapid convergence, and because the corresponding Hessian has a much smaller dimension.

(d) The INMA protocol suggested above neglects the kinetic couplings between the degrees of freedom of the solute and those of the solvent, which can be included upon joint minimization.[14] However, as stated already further above, the effects of these couplings have been shown to be negligible for calculated frequencies and to be small for intensities.[14] Thus, for reasons of computational feasibility, this approximation appears to be justified.

As a result, it remains to be shown whether the two protocols render comparable results for the computation of the vibrational spectra of molecules in solution. As our sample molecule, we will choose *p*-benzoquinone dissolved in pure liquid water, (i) because it is the chemically most simple prototype of the biologically important quinones addressed above, (ii) because the accurate computation of its gas-phase IR spectra by DFT methods is well established,[9,16,6] and (iii) because one can expect that its C═O and C═C modes will be sizeably affected by electrostatic interactions with the strong water dipoles (i.e., by hydrogen bonding).

The fact mentioned in point (ii) above that DFT can provide excellent intramolecular force fields for quinones has first been demonstrated for *p*-benzoquinone.[9,16] Here, the gradient-corrected exchange functional of Becke[17] and the correlation functional of Perdew[18] together with a Gaussian 6-31G** basis set[19] comprising *d* and *p* polarization functions have been shown to yield harmonic frequencies for the C═O and C═C modes, which quantitatively reproduce gas-phase observations and render scaling procedures superfluous. We will denote this DFT method, which also yields high-quality harmonic force fields for a large class of other molecules,[10] as BP86/6-31G**.

Unfortunately, we will not be able verify the sizable solvation effects expected in point (iii) for the C═O modes of *p*-benzoquinone by comparison with IR spectra, because such spectra (as opposed to Resonance Raman spectra) are unknown to us. Therefore, our computational results will represent predictions in this respect.

First estimates on the sizes of the expected band shifts can be obtained from calculations on small, rigid quinone−water clusters. Previous calculations of this type have solely studied *structural* changes of *p*-benzoquinone upon hydrogen bonding.[20] However, because cluster calculations do not treat a quinone in liquid water at room temperature, they cannot fully explain the corresponding IR spectra. Therefore, we will use cluster computations mainly for the evaluation and distinction of various computational methods. To actually calculate the IR spectra we will dissolve *p*-benzoquinone in a periodic cube of MM water molecules and run a QM/MM dynamics simulation at 300 K.

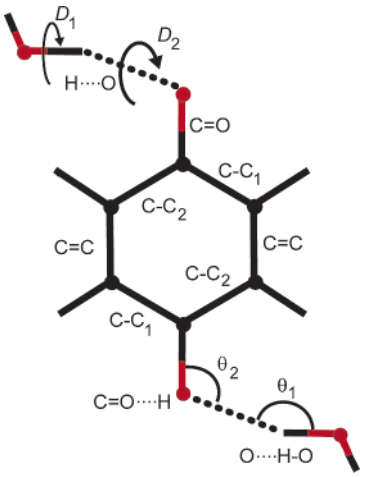

Figure 1. Structure of a small *p*-benzoquinone−water cluster. Also indicated are various geometrical parameters.

The IR spectra will then be derived by FTTCF and INMA protocols and will be compared for evaluation of merits and deficiencies.

2. Computational Methods

Our QM/MM calculations have been carried out with the MD program package EGO-MMII,[21] into which the DFT program CPMD[22] has been integrated for the treatment of the QM-fragments as described by Eichinger and collaborators.[8] Because CPMD employs a plane-wave basis set and pseudopotentials accounting for the core electrons, we have to check corresponding descriptions by comparisons with the established all-electron BP86/6-31G** method. For this purpose, we will use vacuum calculations on *p*-benzoquinone with or without a few surrounding water molecules.

To generate the BP86/6-31G** references for these test calculations, we have used GAUSSIAN98.[23] We have conducted tests for the CPMD implementation of the BP86 functional, which is here combined with the normconserving pseudopotentials of Troullier and Martins.[24] This method, which we denote by MT/BP, requires a plane-wave cutoff measuring at least 70 Ry.[25] Further tests pertain to a computationally much less expensive alternative provided by CPMD. This method combines the super-soft Vanderbilt pseudopotentials[26] with the local density approximation,[27] will be denoted as VDB/LDA, and allows a cutoff as small as 25 Ry.[28] Due to the correspondingly small plane wave basis set, the computational effort is small enough to enable extended QM/MM dynamics simulations.

For the tests, two vacuum models have been studied: Isolated *p*-benzoquinone and the small cluster depicted in Figure 1, in which each of the *p*-benzoquinone carbonyl groups is hydrogen bonded to a water molecule. Whereas the DFT structure and normal mode calculations on isolated *p*-benzoquinone solely serve for a comparison of the three QM methods BP86/6-31G**, MT/BP and VDB/LDA, the cluster calculations additionally aim at the test of a QM/MM hybrid description, in which the QM-fragment is treated by the computationally most efficient VDB/LDA method.

Within the (VDB/LDA)/MM description, the cluster is partitioned into an MM-fragment comprising the two water molecules and a QM fragment covering *p*-benzoquinone. For the MM water molecules, we have chosen the simple TIP3P (three point transferable intermolecular potential) force field.[29] However, in contrast to the original TIP3P model, the water molecules were allowed to be completely flexible. The required force constants, partial charges, and Lennard-Jones parameters have been taken from the CHARMM19 force field.[30,31] In the QM/MM setting, Lennard-Jones potentials are also required for the C-, O-, and H-atoms of *p*-benzoquinone to avoid the intrusion of the water molecules into the space filled by the electronic wave function. Like in CHARMM,[31] we derive these pair potentials from atom-type specific parameters ϵ and σ, specifying their depths and zero crossings. We have chosen the ϵ-values 0.0903, 0.0498, and 0.2342 kcal/mol and the σ-values 3.2072, 1.4254, and 2.6406 Å for C, H, and O, respectively.[32]

With the pure QM Hamiltonians, and in the case of the cluster, also with the (VDB/LDA)/MM Hamiltonian, the minimum energy coordinates and corresponding Hessians of the two vacuum models were calculated. Note that the Hessians were always restricted to the benzoquinone entailing a neglect of kinetic couplings with the water molecules in the cluster (cf. the above discussion). The benzoquinone normal modes and frequencies were derived in the usual way. For the MT/BP method, frequencies were scaled by a factor of 1.0122 obtained from a matching of computational results to experimental data.[6] All other frequencies are unscaled.

For the computation of the IR solution spectra, a $(46.6\ \text{Å})^3$ a periodic box was filled with 3365 flexible TIP3P water molecules surrounding the *p*-benzoquinone, which was treated by the efficient VDB/LDA method. The required MM parameters were chosen as described above for the (VDB/LDA)/MM cluster. For further details on the QM/MM interface, we refer to Eichinger and co-workers.[8] Within the whole system, the long-range Coulomb interactions have been treated by the moving-boundary reaction field (MB/RF) approach of Mathias et al.,[11] with a dielectric boundary 21 Å distant from each molecule. Within that boundary, the electrostatics has been treated explicitly using structure-adapted multipole expansions.[33,34] Here, the Coulomb sum was employed for the atomic partial charges up to a distance of 10 Å. Beyond this distance, the electrostatics was computed by multipole expansions of the partial charge distributions within the water and quinone molecules.

The density of the solvent was set to the experimental density of water at 300 K and the simulations were carried out in the *NVT* ensemble. The temperature was controlled through coupling to an external heat bath[35] (coupling time constant $\tau = 0.1$ ps, target temperature $T_0 = 300$ K). Only the MM atoms were coupled to the heat bath, whereas the QM atoms were exclusively driven by the Newtonian dynamics. With this provision, we wanted to avoid that the time correlation functions of the quinone are directly affected by the thermostat. Indirect influences mediated by the surrounding MM solvent molecules cannot be completely excluded. However, they should be negligibly small, because the algorithmic noise heating the system is very small in the chosen MB/RF method for a system of the given considerable size,[11] and because, therefore, the influence the thermostat on the individual MM atoms becomes extremely small.

A short time step of 0.25 fs was used in all simulations. A multiple time step procedure was applied to the integration of the Newtonian equations.[36,8] After a short MM equilibration (11 ps) at 300 K with an approximate MM force field for quinone derived from vacuum BP86/6-31G** calculations (partial charges, force constants) we switched to the (VDB/LDA)/MM force field and continued to equilibrate the system for another 7.5 ps. Finally, a 17.5 ps (VDB/LDA)/MM trajectory was run for analysis. Although this trajectory is relatively short, it

nevertheless represents a considerable amount of computer time, which is almost exclusively consumed for the VDB/LDA computations (equivalent to three years on a single Compaq XP1000 work station).

According to the FTTCF theory, the infrared absorption coefficient $\alpha(\omega)$ is calculated from a dynamics trajectory of the quinone dipole moment $M(t)$ obtained by DFT according to

$$\alpha(\omega) = \frac{4\pi\omega \tanh(\hbar\omega/2kT)}{3\hbar n(\omega)cV} \cdot \int_{-\infty}^{+\infty} dt e^{-i\omega t}\langle M(t) \cdot M(0)\rangle$$

where $n(\omega)$ is the refractive index, c is the speed of light, and V is the volume of the system.[37] However, in practice, the infinite time-integral in this Fourier transformation of the dipole moment autocorrelation function $\langle M(t) \cdot M(0)\rangle$ can only be executed over the limited time span covered by the simulation. In fact, our 17.5 ps trajectory turned out to be too short for a reliable evaluation of this expression by direct Fourier transformation. Instead, we had to resort to a maximum entropy method.[38] Here, the inverse Fourier transform of a parametric estimate for $\alpha(\omega)$, which is composed of a predefined number of Gaussian IR peaks, is matched to $\langle M(t) \cdot M(0)\rangle$ as calculated from the simulation. For the computation of the spectra according to this method, we have chosen the last $2^{16} = 65536$ time steps of the trajectory corresponding to 16.384 ps. Thus, with our 0.25 fs time step, the autocorrelation functions are sampled at 32768 points and span delay times up to 8.192 ps. The calculated spectrum then covers the frequency range between 0 and 128 000 cm^{-1}. Due to the limited time span of the simulation, the resolution is only about 4 cm^{-1}, as is dictated by Nyquist's theorem. The sole parameter of the maximum entropy modeling[38] is the order M of the approximation, which represents an estimate for the maximum number of peaks expected in the spectrum. We have chosen the value $M = 4096$, because the results turned out to be quite stable upon small variations of M around this value (despite a sizable smoothening of the FTTCF spectra at this value). Parameters M smaller by a factor of 4 resulted in spectra too strongly smoothened, values of M larger by a factor of 4 tended to yield many artificial peaks. Note that the computed spectra show no peaks at all in the huge range above 3500 cm^{-1}.

For an assignment of the IR bands found in this way within the frequency range from 1550 to 1750 cm^{-1}, we have also determined the autocorrelation functions of symmetric and antisymmetric linear combinations of the C═C and C═O bond lengths. Application of the maximum entropy method then yielded the FTTCF spectra of the respective approximate normal coordinates.

To obtain an IR solution spectrum by INMA we have selected seven snapshots from the 17.5 ps (VDB/LDA)/MM trajectory at temporal distances of 2.5 ps. This sizable time lag has been chosen as to approximately guarantee their statistical independence (cf. point (b) in Sec. 1). The small size of the snapshot ensemble will cause certain errors in the computation of expectation values such as mean values or standard deviations. However, for a larger ensemble, a correspondingly extended trajectory would have had to be calculated, which was computationally not feasible for us in a QM/MM setting. A much less costly variant of our INMA approach, in which the MD trajectory for generating an ensemble of solvent shell structures is calculated in a pure MM setting, is yet to be established. Here, we did not choose this approach, because our main focus was the comparison of FTTCF and INMA, into which we did not want to introduce additional parameters such as those of a classical quinone force field or of a different trajectory. As sketched in points (b) and (c) of Section 1, we have minimized the (VDB/LDA)/MM energy with respect to the quinone coordinates for each frozen solvent cage and have determined the corresponding Hessian, normal modes, and IR line spectrum. Subsequently, for each mode, the average $\bar{\nu}$ and the standard deviation σ of the frequency were calculated, which allowed us to construct normalized Gaussian band shapes accounting for the inhomogeneous broadenings. Finally, to generate an INMA solution IR spectrum, the average IR intensities were also calculated and multiplied with the Gaussians.

To check to what extent hydrogen bonds between the water molecules and the quinone C═O groups are formed, the trajectory is analyzed using an empirical energy function provided by the MM/MD program X-PLOR.[39] This energy function measuring the stability of hydrogen bonds is given by

$$E_{\mathrm{Hb}}(d,\theta_1,\theta_2) = \left(\frac{A}{d^6} - \frac{B}{d^4}\right)\cos^4(\theta_1)\cos^2(\theta_2) \qquad (1)$$

Here, the parameters A and B are given through the minimal energy $E_m = -4.25$ kcal/mol at the optimal distance $d_m = 2.75$ Å by $B = -3E_m d_m^4$ and $A = 2Bd_m^2/3$. In a C═O···H−O−H hydrogen bond, d is the distance O···H, θ_1 is the angle O···H−O, and θ_2 is the angle C═O···H (cf. Figure 1). If one of these angles is smaller than an angular cutoff of 90°, the cosines are set to zero. Note that the maximal absolute value $|E_m|$ of E_{Hb} is assumed at a completely collinear C═O···H−O configuration, which may be frequent for strong hydrogen bonds in proteins, but most likely is rare in liquid water, because here a C═O group can form hydrogen bonds to more than one water molecule. Nevertheless, this function can provide estimates on hydrogen bonding.

3. Results and Discussion

First, we want to address the question of how two of the DFT methods provided by CPMD (MT/BP and VDB/LDA) perform in the description of the *p*-benzoquinone force field. We will start by comparing the optimized structures obtained by these methods for isolated *p*-benzoquinone with corresponding results of the BP86/6-31G** reference calculation. To analyze the description of hydrogen bonding by the various DFT methods, we will then turn to the small quinone-water cluster depicted in Figure 1. Here, the DFT geometries will be compared among each other and with the geometry predicted by the (VDB/LDA)/MM hybrid method. Subsequently, these tests will be complemented by a similar analysis of the vibrational spectra, into which we will also introduce available spectroscopic evidence.

Having gained insights into the properties of the computational methods, we will turn to the (VDB/LDA)/MM hybrid MD results on *p*-benzoquinone in water. Here, we will first discuss the quinone structure and the fluctuations of hydrogen bonding, before addressing the quinone C═O and C═C modes obtained by FTTC and INMA, respectively.

3.1. Structures of *p*-Benzoquinone and of a Small Quinone−Water Cluster. Table 1 lists the optimized geometries of isolated *p*-benzoquinone and of the quinone−water cluster as computed by the BP86/6-31G** reference, by MT/BP, and by VDB/LDA. The cluster geometry has been additionally obtained by the (VDB/LDA)/MM hybrid method. The geometrical parameters are defined in Figure 1. Also given are the binding energies E_b per water molecule in the cluster.

For the isolated *p*-benzoquinone, MT/BP agrees quite well with the BP86/6-31G** reference concerning the C═O, C═C,

TABLE 1: Calculated Geometries of Isolated *p*-Benzoquinone and of a Quinone−Water Cluster Using Different Computational Methods[a]

method	system	C═O	C═C	C−C	H···O	D_1	D_2	θ_1	θ_2	E_b
BP86/6-31G**	*p*-benzoquinone	1.239	1.355	1.490						
	cluster	1.247	1.355	1.485/1.488	1.965	92	14	158	112	−8.4
MT/BP	*p*-benzoquinone	1.238	1.345	1.483						
	cluster	1.244	1.346	1.479/1.481	1.952	144	6	159	115	−5.4
VDB/LDA	*p*-benzoquinone	1.258	1.346	1.467						
	cluster	1.267	1.348	1.462/1.468	1.682	176	4	157	111	−12.9
(VDB/LDA)/MM	cluster	1.262	1.348	1.465/1.468	1.866	175	1	147	112	−9.4

[a] Bond lengths are given in Å, the angles D_1, D_2, θ_1, and θ_2 in degrees (see Figure 1 for the definition of the geometrical parameters), and the binding energy E_b per H_2O molecule in kcal/mol.

and C−C bond lengths. The deviations measure at most 0.01 Å. Slightly larger deviations of at most 0.02 Å are found for the much less elaborate VDB/LDA method. Here, the C═O bond is longer, whereas the C═C and C−C bonds are shorter than in the two BP86 descriptions, suggesting that VDB/LDA underestimates the C═O and overestimates the C═C and C−C force constants.

Hydrogen bonding with the two water molecules mainly results in an elongation of the C═O bonds. In the pure DFT treatments, this elongation is 0.008 (BP86/6-31G**), 0.006 (MT/BP), and 0.009 Å (VDB/LDA), which agrees with previous calculations.[20] The pronounced elongation in VDB/LDA further enhances the overestimate of the C═O bond lengths already present in the corresponding treatment of the isolated *p*-benzoquinone. According to the (VDB/LDA)/MM hybrid calculation, this elongation is much smaller, measuring only 0.004 Å. As a result, in the cluster, the VDB/LDA overestimate of the C═O bond lengths becomes smaller by 0.005 Å when switching to the (VDB/LDA)/MM hybrid description. The reduction of the VDB/LDA overestimate indicates that the (VDB/LDA)/MM hybrid method may heal certain shortcomings of VDB/LDA in the description of the cluster.

The latter hypothesis is strengthened by considering the O···H distances in the hydrogen bonds between the water molecules and the quinone carbonyl groups (cf. Tab1). Whereas, according to VDB/LDA, these distances are very small at 1.682 Å, they become elongated by nearly 0.2 Å in the (VDB/LDA)/MM hybrid model of the cluster. Here, the resulting O···H distance of 1.866 Å is only slightly smaller than that predicted by MT/BP (1.952 Å) or by the reference (1.962 Å).

These findings on the C═O and O···H distances show that, in fact, the (VDB/LDA)/MM hybrid approach can partially repair a deficiency of the VDB/LDA method occurring in the description of hydrogen bonded molecules. This deficiency is well known, is called *LDA overbinding*, and is characterized by an overestimation of hydrogen bonding energies,[25] which shows up also here in the last column of Table 1. VDB/LDA assigns an absolute value $|E_b|$ of 12.9kcal/mol to the binding energy per water molecule, which is reduced to 9.4kcal/mol in (VDB/LDA)/MM. This value is quite close to the one predicted by BP86/6-31G** (8.4kcal/mol) but larger than the MT/BP value of 5.4kcal/mol. Calculations on the water dimer have shown that gradient corrected functionals tend to underestimate hydrogen bonding energies,[8] as they cannot account for the dispersion interaction of nonbonded molecules. Because in QM/MM hybrid methods this interaction is empirically included through the use of Lennard-Jones potentials, it may well be that (VDB/LDA)/MM is even better than MT/BP or BP86/6-31G** concerning, for instance, the binding energies or the O···H distances. Note that in the QM/MM setting these values could be further optimized by a tuning of the Lennard-Jones parameters attached to the QM atoms of the quinone. Such tuning would also affect the angle θ_1 (O···H−O), which in (VDB/LDA)/MM is by about 10° smaller than in the DFT treatments (cf. Table 1; in contrast, θ_2 is nearly identical in all descriptions). However, due to the lack of experimental data, we did not pursue this possibility.

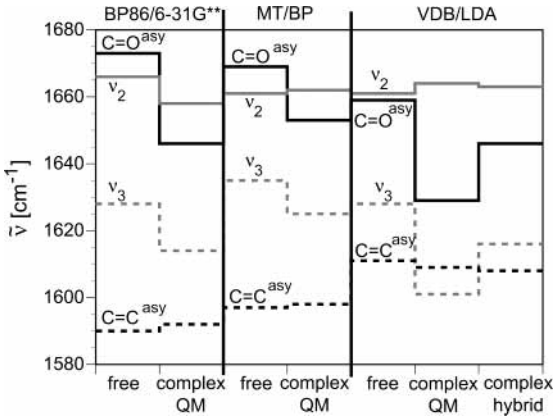

Figure 2. Vibrational frequencies of the C═O and C═C modes in isolated *p*-benzoquinone ("free") and in the quinone-water cluster ("complex") depicted in Figure 1 obtained by three different DFT methods, and for the cluster, also by the (VDB/LDA)/MM hybrid approach.

Concerning the orientations of the water molecules with respect to the quinone, a consideration of the dihedral angles D_1 and D_2 in Tab1 reveals large differences. According to BP86/6-31G** the planes of the water molecules are nearly perpendicular to the quinone plane, MT/BP predicts only small angles, and VDB/LDA describes the molecules as nearly coplanar. In this respect, the QM/MM approach gives the same results as its parent QM method VDB/LDA. Which of the three possibilities is true is unknown. However, we would like to remark that in this respect, the MT/BP result might be even more reliable than that of BP86/6-31G**, because the plane-wave method MT/BP lacks the so-called basis-set superposition error[40] hampering the application of Gaussian based DFT methods to nonbonded systems.[25]

Summarizing this discussion, we may state that the most simple and cost-effective (VDB/LDA)/MM method has shown a surprisingly good performance concerning the structure of the hydrogen bonded cluster, as it has rendered a geometry close to that of MT/BP. This good performance has been explained by the fact that DFT/MM approaches can repair those deficiencies of DFT methods, like the LDA/VDA overbinding or the lack of the attractive dispersion interaction, which hamper DFT descriptions of nonbonded molecular clusters.

3.2. C═O and C═C Vibrational Modes of *p*-Benzoquinone and of a Small Quinone−Water Cluster. Figure 2 displays a term scheme for the frequencies of the four C═O and C═C modes of *p*-benzquinone and of the small quinone−water cluster depicted in Figure 1. The scheme has been computed from

Hessian matrices by the four methods under investigation. We exclusively concentrate on the C═O and C═C modes, because they dominate the quinone vibrational spectra and are strongly affected by hydrogen bonding.

Consider first the frequencies calculated by the pure DFT methods for isolated *p*-benzoquinone, which are displayed in the first, third, and fifth columns of the term scheme. These and further data, comparisons with gas phase observations,[41,42] and an evaluation of these comparisons have already been published.[6] However, because these results are important in the present context, they have to be shortly summarized.

As recently demonstrated,[6] the properly scaled MT/BP frequencies (third column) match the experimental data (not shown) even better than the unscaled BP86/6-31G** results (first column), whose good quality had been noted long ago.[9] The mean square deviations of the computed frequencies from the experimental data are only 4 cm^{-1} for scaled MT/BP and 7 cm^{-1} for BP86/6-31G**. The MT/BP term scheme reveals that the anti-symmetric C═O stretching mode, which is associated with the most intense band in the IR spectrum, has the highest frequency (MT/BP, 1669 cm^{-1}; exp, 1666 cm^{-1}) of the four modes considered. The mode of lowest frequency (MT/BP, 1597 cm^{-1}; exp, 1592 cm^{-1}) belongs to the antisymmetric C═C stretch and gives rise to a much weaker IR band. In the two symmetric modes ν_2 and ν_3, the C═O and C═C stretches are strongly coupled.[6] These modes are symmetry forbidden in IR and allowed in Resonance Raman. They are located in the spectral region between the antisymmetric modes (ν_2 (MT/BP, 1661 cm^{-1}; exp, 1665 cm^{-1}); ν_3 (MT/BP, 1635 cm^{-1}; exp, 1639 cm^{-1})). Therefore, the MT/BP term scheme can be considered as an excellent representation of the experimental data.[6]

For the symmetric modes ν_2 and ν_3, the VDB/LDA method predicts unscaled frequencies (fifth column of Figure 2), which are quite close to the MT/BP results, and consequently, to the experimental findings. However, the antisymmetric C═O stretch is shifted by about 10 cm^{-1} to the red and the C═C stretch by about 20 cm^{-1} to the blue. These shifts corroborate the suggestion derived from the analysis of the bond lengths in Table 1 that VDB/LDA slightly underestimates the C═O and overestimates the C═C force constants. Although these small deficiencies do not affect the frequencies of the symmetric modes, they alter their mode compositions.[6]

These results suggest that one should replace unscaled BP86/6-31G** by scaled MT/BP whenever a reference method for the computation of quinone force fields is required. Consequently, an (MT/BP)/MM combination had been applied to compute the IR spectra of the two *ubiquinones*, Q_A and Q_B, in the photosynthetic reaction center of *Rb. sphaeroides*.[6] The apparent success of this (MT/BP)/MM hybrid approach (cf. Sec. 1) strengthens the above suggestion. Therefore, we will consider from now on vibrational spectra derived by scaled MT/BP as a reference in all cases, in which experimental data are not available. Only occasionally will we still use the previous reference (i.e., BP86/6-31G**). However, the results suggest in addition that the computationally much more efficient VDB/LDA method can provide at least reasonable quinone force fields. It remains to be seen whether the improvement of descriptions, which we have noted for the (VDB/LDA)/MM hybrid method in connection with the quinone geometries in the hydrogen bonded cluster, show up also in the vibrational spectra. Therefore, we now turn to the vibrational spectra of *p*-benzoquinone in this cluster.

In Figure 2, the columns two (BP86/6-31G**), four (scaled MT/BP), and six (VDB/LDA) exhibit the term schemes computed for the C═O and C═C modes of *p*-benzoquinone surrounded by two water molecules. To highlight the effects of hydrogen bonding, the mode frequencies in the cluster are linked to the corresponding frequencies of the isolated quinone in the preceding columns.

According to all descriptions, the hydrogen bonds strongly red-shift the antisymmetric C═O mode and leave the antisymmetric C═C mode nearly invariant. Also, for the symmetric mode ν_3, sizable red-shifts are predicted. The directions and sizes of the shifts computed for ν_2 vary with the respective method but are always smaller than those for ν_3. Comparing the resulting BP86/6-31G** and VDB/LDA frequencies with those obtained by the MT/BP reference model we find mean square deviations of 11 cm^{-1} (BP86/6-31G**) and 22 cm^{-1} (VDB/LDA), respectively. Thus, pure VDB/LDA definitely represents a very bad approximation to the best available frequency estimate provided by MT/BP.

As compared to MT/BP, pure VDB/LDA assigns a very low frequency to the asymmetric C═O stretch, which is another consequence of the LDA overbinding and finds a correspondence in the strong VDB/LDA elongation of the C═O bond upon hydrogen bonding (cf. Section 3.1). According to VDB/LDA, the symmetric mode ν_3, which is dominated by the symmetric C═O stretch, is also strongly red-shifted to 1601 cm^{-1} and becomes the mode of lowest frequency.

Fortunately, these deficiencies are largely repaired in the transition from the VDB/LDA to the (VDB/LDA)/MM description of the cluster. As shown by the term scheme in the last column of Figure 2, the frequency ordering of the vibrational modes becomes correct, and all frequencies shift toward the MT/BP reference locations. The mean square deviation of the (VDB/LDA)/MM frequencies from the MT/BP reference values is only 11 cm^{-1} (i.e., it is as small as the deviation of BP86/6-31G**). Note that we have also carried out a scaled (MT/BP)/MM hybrid calculation of the cluster (data not shown), which deviates from the reference also, by 12 cm^{-1}. Furthermore, we have checked that the relative intensities of the two antisymmetric modes are nearly invariant in the transition from a purely quantum mechanical treatment (MT/BP and VDB/LDA) of the cluster to the (VDB/LDA)/MM description. As a result, in a QM/MM setting the use of VDB/LDA instead of MT/BP saves a huge amount of computer time without sacrificing too much of the accuracy achievable in computations of vibrational spectra.

Here, the final question arises as to what extent cluster calculations can describe observed solvent shifts. Experimental data for solvation in water are solely available for the Raman active mode ν_2. For this mode, a slight blue shift from the gas-phase value of 1661−1668 cm^{-1} has been observed.[42] According to Figure 2, the ν_2-frequency of the cluster is slightly shifted to the blue (compared to the isolated molecule) both in the MT/BP and (VDB/LDA)/MM descriptions with ν_2-frequencies resulting at 1661 and 1663 cm^{-1}, respectively.

All our cluster calculations agree that the antisymmetric C═C mode should be insensitive to solvation effects, which is why we would expect the corresponding solution IR band near the gas-phase frequency of 1592 cm^{-1}.[41] From the (VDB/LDA)/MM cluster prediction of 1608 cm^{-1}, we therefore are lead to assume that this frequency will also be overestimated by our (VDB/LDA)/MM dynamics simulation.

Because the cluster calculations predict that the remaining two modes ($C{=}O^{asy}$ and ν_3) are very sensitive to hydrogen bonding, sizable shifts in polar solvents are to be expected. Unfortunately, for water, corresponding data are lacking. Such

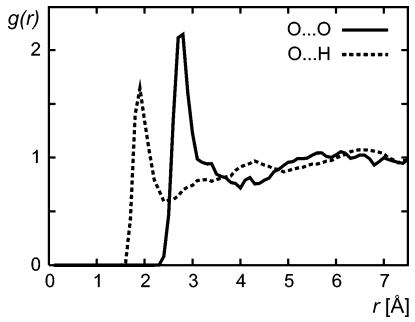

Figure 3. Radial distribution functions g_{OH} and g_{OO} of the H_2O hydrogen and oxygen atoms, respectively, around the oxygen atoms of the *p*-benzoquinone C═O groups calculated from the 17.5 ps QM/MM trajectory using a bin size of 0.1 Å.

data are only available for other solvents (CCl_4, $CHCl_3$, and *n*-hexane) of varying polarity.[43] For C═O^{asy}, the solvation in CCl_4 and $CHCl_3$ entails red-shifts of 3 and 6 cm^{-1}, respectively. To check the cluster description of solvation, we have carried out additional BP86/6-31G** test calculations on clusters, in which the two water molecules were replaced by CCl_4 and $CHCl_3$, respectively. As compared to the BP86/6-31G** description of the isolated molecule, in these clusters, the C═O ^{asy} frequency was red-shifted by 13 cm^{-1} (CCl_4) and 15 cm^{-1} ($CHCl_3$). These shifts are much larger than observed. This seems to suggest that cluster calculations may not represent quantitative models for solvation effects and points to the importance of solvent simulations.

3.3. The Structure of *p*-Benzoquinone in Water from a QM/MM MD Simulation. Using VDB/LDA for *p*-benzoquinone and the TIP3P force field for the surrounding water molecules we have run the 17.5 ps QM/MM dynamics simulation described in Section 2. From the trajectory, we have determined the average geometry of the quinone. For the bond lengths, we found the values 1.265 ± 0.008 Å (C═O) and 1.348 ± 0.007 Å (C═C). As compared to the (VDB/LDA)/MM geometry of the cluster, the mean C═O bond length is elongated by 0.003 Å, whereas the mean C═C bond length is identical (cf. Table 1). This suggests that in the aqueous solution, the additional elongation of the C═O bonds is caused by the formation of hydrogen bonds, which are stronger than in the cluster. Correspondingly, one expects an enhanced red-shift of the C═O modes.

To provide insight into the hydrogen bonding between the water molecules and the quinone C═O groups, Figure 3 shows the radial distribution functions $g_{OH}(r)$ and $g_{OO}(r)$ of the H_2O hydrogen and oxygen atoms, respectively, around the oxygen atoms of the quinone C═O groups as calculated from the QM/MM trajectory. The two functions exhibit pronounced peaks at 1.9 Å and 2.8 Å, respectively. Within the limited resolution of the distribution functions, these peak positions agree very well with the corresponding equilibrium distances in the cluster, which are 1.866 Å (O···H) and 2.731 Å (O···O) according to the (VDB/LDA)/MM treatment. These pronounced peaks indicate that the C═O oxygen atoms are surrounded by a distinct first solvation shell of water molecules. Taking the first minimum at $r = 2.5$ Å of $g_{OH}(r)$ as a clue to the boundary of this shell, one finds by integration that it contains three hydrogen atoms. Three oxygen atoms are covered by the first peak of $g_{OO}(r)$ up to $r = 3$ Å. This suggests that on the average three water molecules form hydrogen bonds with each C═O group.

This result is at variance with classical MD simulations on *p*-benzoquinone in water,[44] according to which (i) the first peak of $g_{OH}(r)$ at 1.9 Å has only half the height of the one shown in Figure 3 (cf. Figure 1 in ref 44), and (ii) $g_{OO}(r)$ is essentially constant at the value one after the onset at 2.5 Å (cf. Figure 2 in ref 44). Thus, according to the MM simulation, the first hydration shell is missing. A key difference between our QM/MM treatment and the MM-MD simulation is that we include the polarizability of *p*-benzoquinone, whereas the MM approach applies static partial charges. Due to its conjugated π-electron system, *p*-benzoquinone should be strongly polarizable. Thus, the local dipoles in the C═O groups can be enhanced by H_2O molecules forming hydrogen bonds, which effect can stabilize these hydrogen bonds.

Here, we have asked the question of whether all three water molecules in the first hydration shell are actually involved in hydrogen bonding. For an answer we have selected all water molecules that have visited the first hydration shell during the 17.5 ps MD-simulation. To these H_2O molecules we have applied the empirical energy function E_{Hb} given by eq 1, sampling the trajectory at a rate of 2.5 fs. Next we have selected all those H_2O molecules for which $E_{Hb}(d,\theta_1,\theta_2)$ is smaller than −0.001kcal/mol during a period exceeding 10 fs. We found that 21 different H_2O molecules per C═O group are selected by these criteria and that at each point of time on the average 2.3 of the three H_2O molecules are involved in hydrogen bonding. The average energy $\langle E_{Hb}\rangle = -0.58$kcal/mol per hydrogen bond is nearly twice the hydrogen bonding energy $E_{Hb} = -0.30$kcal/mol in the (VDB/LDA)/MM cluster geometry. This indicates stronger hydrogen bonding in solution as compared to the static cluster calculation. The energy weighted average hydrogen bonding energy $\langle E_{Hb}^2\rangle/\langle E_{Hb}\rangle = -1.49$kcal/mol shows that, occasionally, very strong hydrogen bonds are formed.

The average lifetime of a hydrogen bond is 0.16 ps. Because only 21 molecules form hydrogen bonds during the 17.5ps trajectory, this short lifetime cannot be associated with a diffusive exchange in and out of the hydration shell but must be due to a rapid hydrogen bonding exchange among the three H_2O molecules within that shell. Therefore, the 21 H_2O molecules determined as hydrogen partners of a C═O group are also all H_2O molecules that occupy the first hydration shell within the simulation. Now one immediately concludes that each of the three members of the shell is exchanged seven times during the 17.5 ps, which yields a lifetime of 2.5 ps for a water molecule within the shell.

Therefore, in the liquid, the elongation of the C═O bond (compared to the small static cluster) noted above is due to the concerted action of 2.3 hydrogen bonds. Furthermore, the rapid 2.5 ps exchange of water molecules that form hydrogen bonds with the C═O groups suggests that the INMA sampling time lags of 2.5 ps are large enough for generating a statistically independent snapshot ensemble.

3.4. The Infrared Spectrum of *p*-Benzoquinone in Water. Figure 4 compares the IR spectrum obtained from the autocorrelation function of the dipole moment (thick black solid line) with the FTTCF spectra of the approximate normal modes (see Sect. 2). Four maxima at 1608 cm^{-1}, 1642, 1678, and 1740 cm^{-1} are seen in the IR spectrum. As mentioned in Section 2, the small time span of the simulation limits the resolution of this spectrum to 4 cm^{-1}. However, because the applied maximum entropy method introduces a smoothening, the resolution is further reduced.

The FTTCF spectra of the anti-symmetric and symmetric C═O and C═C normal modes have a much simpler structure than the IR spectrum, as they all have only one large maximum. For the IR active anti-symmetric modes (solid lines), these maxima are located at 1642 cm^{-1} (C═O^{asy}, gray) and at 1608

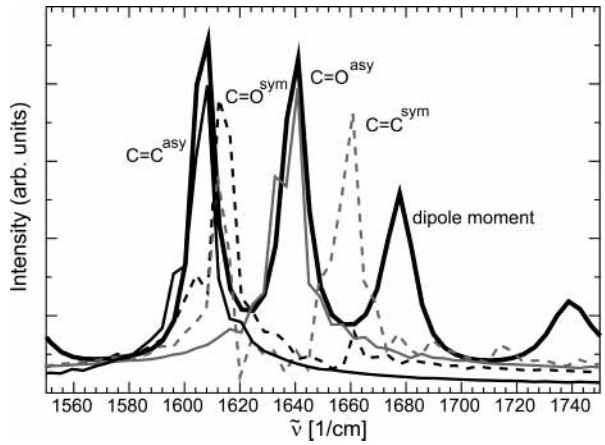

Figure 4. The IR spectrum of *p*-benzoquinone in water calculated from the autocorrelation function of the dipole moment (thick black solid linestyle) is compared to the FTTCF spectra of approximate C═O and C═C normal modes (C═O^{asy}, thin gray; C═C^{asy}, thin black; $\nu_3 \equiv$ C═O^{sym}, dashed thin black; $\nu_2 \equiv$ C═C^{sym}, dashed thin gray).

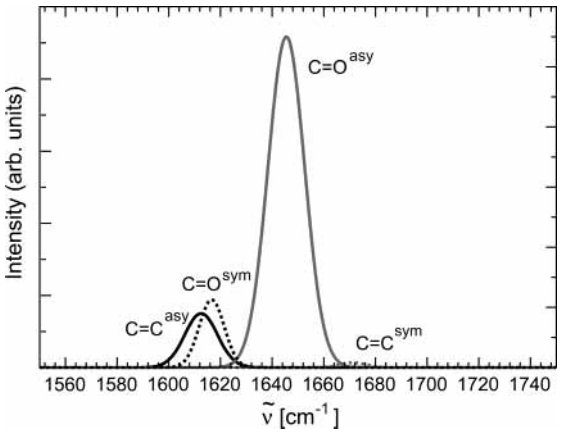

Figure 5. IR spectrum of *p*-benzoquinone in water constructed from snapshots of the (VDB/LDA)/MM simulation by the INMA procedure. For explanations, see the text.

cm^{-1} (C═C^{asy}, black). For the Raman active symmetric modes (dashed lines), they are found at 1661 cm^{-1} ($\nu_2 \equiv$ C═C^{sym}, gray) and at 1612 cm^{-1} ($\nu_3 \equiv$ C═O^{sym}, black).

Therefore, the bands at 1642 and 1608 cm^{-1} in the FTTCF IR spectrum can be assigned to the IR active anti-symmetric C═O and C═C combinations, respectively. The exact matching of the FTTCF band positions as derived from two different observables, from the DFT dipole moment $M(t)$ and from the DFT bond lengths projected on approximate normal coordinates, suggests that the FTTCF method actually determines the band positions at the accuracy given by the resolution of $\pm$ 2 cm^{-1}.

On the other hand, the remaining peaks in the FTTCF IR spectrum are artificial. Simulations with a completely rigid water model (data not shown) have demonstrated that the weak band at 1740 cm^{-1} is absent here. A normal-mode analysis of our flexible TIP3P water model yields this frequency for the H−O−H bending mode. Thus, the 1740 cm^{-1} band in the FTTCF IR spectrum is due to a coupling of the quinone dipole moment with this bending mode of the water molecules. The origin of the band at 1678 cm^{-1}, however, remains unclear. Most likely, it is an artifact of the maximum entropy method, which is connected with the lack of a sufficiently extended trajectory.[45]

Figure 5 shows the IR spectrum of *p*-benzoquinone in water as constructed from the MD trajectory by the INMA procedure described in Sec. 2. The spectrum exhibits a single very intense and broad (σ = 7.1 cm^{-1}) band, which belongs to the anti-

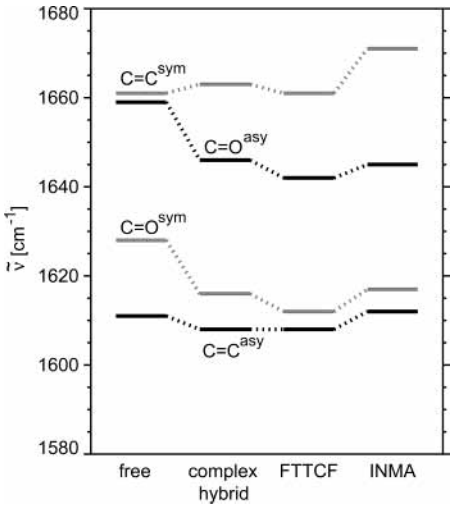

Figure 6. Solvation effects on the C═O and C═C vibrational frequencies. The VDB/LDA results for isolated *p*-benzoquinone ("free") are compared with the (VDB/LDA)/MM frequencies obtained for the quinone−water cluster ("complex hybrid") and with the FTTCF and INMA solution data. For explanations, see the text.

symmetric C═O stretch and is centered at 1645 cm^{-1}. This band is about seven times more intense than that of the anti-symmetric C═C stretch at 1612 cm^{-1}, which is sharper (σ = 6.4 cm^{-1}) and that of the symmetric C═O stretch (ν_3) at 1617 cm^{-1}, which is much sharper (σ = 4.9 cm^{-1}). The intensity of the rather sharp (σ = 5.1 cm^{-1}) band at 1671 cm^{-1}, which belongs to the symmetric C═C stretch (ν_2), is very small (i.e., by about a factor of 100 smaller than that of the most intense anti-symmetric C═O stretch). The fact that also the symmetric modes gain some intensity is due to the broken symmetry of *p*-benzoquinone in the solvent cages. Note that the inhomogeneous line widths correlate only for some modes (C═O ^{asy} and ν_2) with the sizes of the spectral shifts caused by hydrogen bonding (cf. Figure 2), whereas for the others they do not.

Figure 6 compares the INMA band positions with the corresponding FTTCF data. To provide insight into the solvation effects on the frequencies, this figure also includes the VDB/LDA results on isolated *p*-benzoquinone and the (VDB/LDA)/MM data on the quinone-water cluster. The depicted comparison of INMA and FTTCF reveals an average blue-shift of the INMA frequencies by 5 cm^{-1}. Thus, the two techniques for calculating the IR spectra of a molecule in solution yield similar but not identical frequencies. Whether these differences are statistically significant is unclear. In both techniques, the accuracy of the results can be strongly enhanced by increasing the database, i.e., by using a much longer trajectory for FTTCF (see Section 2) and a correspondingly larger set of statistically independent snapshots for INMA (cf. Sec.1, points (b) and (c)). An increased database would also enable comparisons of computed band-widths, which are excluded here due to the insufficient resolution of the FTTCF spectra and due to the insufficient statistics of the INMA spectrum. Nevertheless, the reasonable agreement of frequencies indicates that, in principle, both techniques are valid for determining band positions. The INMA technique may even be superior, because here possible artifacts like the unexplained band at 1678 cm^{-1} appearing in the dipole spectrum are lacking. Note that INMA gives a different estimate of the IR intensities than does FTTCF: According to the IR spectrum in Figure 4 the anti-symmetric C═C and C═O modes should have comparable intensities, whereas the spectrum in Figure 5 predicts a much stronger C═O band. Which of the two

alternatives is true remains to be clarified by IR spectroscopy or by more extended calculations.

It is also important to compare the band positions of the solution spectra with those obtained by the same computational method for the small quinone water cluster (cf. Figure 6, "complex hybrid"). Taking the FTTCF data, one finds that the band positions are essentially identical within the 4 cm^{-1} FTTC resolution. The solvent induced band shifts predicted by FTTCF and INMA from the dynamics simulation and by (VDB/LDA)/MM for the static cluster are very close as is apparent by comparison of the first three columns in Figure 6. In the case of INMA, the general 5 cm^{-1} blue-shift with respect to FTTCF slightly modifies this picture as it entails a larger solvation-induced blue-shift for the symmetric C═C stretch than that predicted by the FTTCF and cluster calculations. All three computational approaches toward solvation effects equally predict sizable red-shifts of about 14 cm^{-1} for the two C═O modes. Interestingly, neither FTTCF nor INMA renders an additional red-shift of these modes as compared to the cluster frequencies, which had been suggested by the elongation of the C═O bond observed in the transition from the cluster to the dynamics simulation (cf. Section 3.3). Hence, whereas in static calculations the bond lengths nicely correlate with the corresponding force constants and frequencies, such correlations may be absent when comparing static with dynamics results. Summarizing these comparisons, we conclude that the insufficient accuracy provided by the 17.5 ps trajectory for the FTTCF and INMA solution spectra precludes a final evaluation of the merits of cluster calculations for estimating solvent shifts.

Experimental data, with which one could compare the dynamics results, are sparse. Only for the spectral position of the symmetric C═C mode is the Raman value of 1668 cm^{-1} known to us.[42] This value is in excellent agreement with the 1661 cm^{-1} of FTTCF and 1671 cm^{-1} of INMA.

4. Conclusion

We have explored two different computational protocols, FTTC and INMA, which allow the calculation of the IR spectra of a molecule in solution from QM/MM dynamics simulations. To establish a QM/MM method suitable for the description of quinones in solution, we have first compared and evaluated different DFT methods using isolated *p*-benzoquinone and a small quinone−water cluster as our testing ground. Here, we found that the most simple and computationally efficient VDB/LDA method performs quite well in a QM/MM setting, particularly since (VDB/LDA)/MM can repair shortcomings encountered in pure VDB/LDA treatments of molecular clusters. Having thus established a suitable QM/MM hybrid method for *p*-benzoquinone in liquid water, we have determined its IR spectrum through the autocorrelation functions of its dipole moment and of approximate normal coordinates (FTTCF). Alternatively, we have calculated this spectrum also from a statistics over results of a series of instantaneous normal-mode analyses (INMA), which were executed for structural snapshots of the QM/MM simulation. Concerning vibrational frequencies, the results of both procedures agree within statistical error. Although the 17.5 ps QM/MM-MD trajectory employed by us has been long enough to obtain comparable frequencies and represents a huge computational effort, it has been too short for a detailed comparison of the FTTCF and INMA spectra with respect to the bandwidths and intensities. It seems, however, that INMA can avoid certain artifacts, which may hamper FTTCF.

As far as the *p*-benzoquinone molecule in water is concerned, we found that the single known band position (symmetric C═C stretch) is closely reproduced by the calculations. In disagreement with MM-MD simulations we observed a sizable hydrogen bonding between water and the quinone. Water molecules hydrogen bonded to the quinone C═O groups turned out to exchange rapidly at a time scale of at most 2.5 ps.

Acknowledgment. This work was supported by the *Volkswagen Stiftung* (Project I/73 224) and the *Deutsche Forschungsgemeinschaft* (SFB533/C3). Computer time has been provided by the Leibniz-Rechenzentrum (Project h0431).

References and Notes

(1) Trumpower, B. L. *Function of Quinones in Energy Conservation*; Academic Press: New York, 1982.

(2) Okamura, M. Y.; Paddock, M. L.; Graige, M. S.; Feher, G. *Biochim. Biophys. Acta* **2000**, *1458*, 148−163.

(3) Brudler, R.; de Groot, J.; van Liemt, W.; Steggerda, W.; Esmeijer, R.; Gast, P.; Hoff, A.; Lugtenburg, J.; Gerwert, K. *EMBO J.* **1994**, *13*, 5523.

(4) Breton, J.; Burie, J.-R.; Boullais, C.; Berger, G.; Nabedryk, E. *Biochemistry* **1994**, *33*, 12405.

(5) Breton, J.; Boullais, C.; Berger, G.; Mioskowski, C.; Nabedryk, E. *Biochemistry* **1995**, *34*, 11606.

(6) Nonella, M.; Mathias, G.; Eichinger, M.; Tavan, P. *J. Phys. Chem. B* **2003**, *107*, 316−322.

(7) Warshel, A.; Levitt, M. *J. Mol. Biol.* **1976**, *103*, 227−249.

(8) Eichinger, M.; Tavan, P.; Hutter, J.; Parrinello, M. *J. Chem. Phys.* **1999**, *110*, 10452−10467.

(9) Nonella, M.; Tavan, P. *Chem. Phys.* **1995**, *199*, 19−32.

(10) Neugebauer, J.; Hess, B. A. *J. Chem. Phys.* **2003**, *118*, 7215−7225.

(11) Mathias, G.; Egwolf, B.; Nonella, M.; Tavan, P. *J. Chem. Phys.* **2003**, *118*, 10847−10860.

(12) Ermler, U.; Fritzsche, G.; Buchanan, S. K.; Michel, H. *Structure* **1994**, *2*, 925−936.

(13) Stowell, M. H. B.; McPhillips, T. M.; Rees, D. C.; Soltis, S. M.; Abresch, E.; Feher, G. *Science* **1997**, *276*, 812−816.

(14) Cui, Q.; Karplus, M. *J. Chem. Phys.* **2000**, *112*, 1133−1149.

(15) A solute molecule is exposed to an external electrostatic field generated by the surrounding solvent molecules. The contributions to the field originating from rapid electron density fluctuations in the solvent molecules cause the attractive dispersion interaction. They are approximately homogeneous, isotropic, and are identical in polar and nonpolar solvents. Therefore, they do not specifically change the electron density and the associated force field within the solute. As a consequence, its vibrational modes are hardly affected by solvation in nonpolar solvents. In polar solvents, however, the additional contributions originating from the permanent dipoles in the structured and slowly fluctuating solvent shells add up to the field generated by the nuclei, to which, according to Born−Oppenheimer approximation, the electrons of the solute instantaneously adjust. These added fields generate the electronic polarization, and correspondingly, change the effective electronic potential of nuclear motion.

(16) Boesch, S. E.; Wheeler, R. A. *J. Phys. Chem.* **1995**, *99*, 8125.

(17) Becke, A. D. *Phys. Rev. A* **1988**, *38*, 3098.

(18) Perdew, J. P. *Phys. Rev. B* **1986**, *33*, 8822.

(19) Francl, M.; Pietro, W.; Hehre, W.; Binkley, J.; Gordon, M.; deFrees, D.; Pople, J. *J. Chem. Phys.* **1982**, *77*, 3654.

(20) O'Malley, P. J. *Chem. Phys. Lett.* **1997**, *274*, 251−254.

(21) Mathias, G.; Eichinger, M.; Carstens, H.; Stork, M.; Weiss, A.; Heller, H.; Grubmüller, H.; Egwolf, B.; Niedermeier, C.; Tavan, P. "EGO-MMII users guide", Lehrstuhl für BioMolekulare Optik, Ludwig Maximilian Universität München, Oettingenstrasse 67, D-80538 München, in preparation.

(22) Hutter, J.; Alavi, A.; Deutsch, T.; Bernasconi, M.; Goedecker, S.; Marx, D.; Tuckermann, T.; Parrinello, M. *CPMD*, version 3.4.0, MPI für Festkörperforschung and IBM Zurich Research Laboratory.

(23) Frisch, M. J.; Trucks, G. W.; Schlegel, H. B.; Scuseria, G. E.; Robb, M. A.; Cheeseman, J. R.; Zakrzewski, V. G.; Montgomery, J. A., Jr.; Stratmann, R. E.; Burant, J. C.; Dapprich, S.; Millam, J. M.; Daniels, A. D.; Kudin, K. N.; Strain, M. C.; Farkas, O.; Tomasi, J.; Barone, V.; Cossi, M.; Cammi, R.; Mennucci, B.; Pomelli, C.; Adamo, C.; Clifford, S.; Ochterski, J.; Petersson, G. A.; Ayala, P. Y.; Cui, Q.; Morokuma, K.; Malick, D. K.; Rabuck, A. D.; Raghavachari, K.; Foresman, J. B.; Cioslowski, J.; Ortiz, J. V.; Stefanov, B. B.; Liu, G.; Liashenko, A.; Piskorz, P.; Komaromi, I.; Gomperts, R.; Martin, R. L.; Fox, D. J.; Keith, T.; Al-Laham, M. A.; Peng, C. Y.; Nanayakkara, A.; Gonzalez, C.; Challacombe, M.; Gill, P. M. W.; Johnson, B. G.; Chen, W.; Wong, M. W.; Andres, J. L.; Head-Gordon, M.; Replogle, E. S.; Pople, J. A. *Gaussian 98*, revision A.5; Gaussian, Inc.: Pittsburgh, PA, 1998.

(24) Troullier, N.; Martins, J. *Phys. Rev. B* **1991**, *43*, 1993.
(25) Sprik, M.; Hutter, J.; Parrinello, M. *J. Chem. Phys.* **1996**, *105*, 1142−1152.
(26) Vanderbilt, D. *Phys. Rev. B* **1990**, *41*, 7892.
(27) Parr, R. G.; Yang, W. *Density-functional Theory of Atoms and Molecules*; Oxford University Press: New York, 1989.
(28) Laasonen, K.; Sprik, M.; Parrinello, M.; Car, R. *J. Chem. Phys.* **1993**, *99*, 9081.
(29) Jorgensen, W. L.; et al., *J. Chem. Phys.* **1983**, *79*, 926.
(30) Brooks, B. R.; Bruccoleri, R. E.; Olafson, B. D.; States, D. J.; Swaminathan, S.; Karplus, M. *J. Comput. Chem.* **1983**, *4*, 187.
(31) Neria, E.; Fischer, S.; Karplus, M. *J. Chem. Phys.* **1996**, *105*, 1902−1921.
(32) These parameters were taken from the file parmallh3x.pro contained in the distribution of the MD program XPLOR 3.1 by A. Brünger, The Howard Hughes Medical Institute and Department of Molecular Biophysics and Biochemistry, Yale University, New Haven, 1992. We do not consider the choice of the Lennard-Jones parameters to be critical for our purposes.
(33) Niedermeier, C.; Tavan, P. *J. Chem, Phys.* **1994**, *101*, 734.
(34) Niedermeier, C.; Tavan, P. *Mol. Simul.* **1996**, *17*, 57−66.
(35) Berendsen, H. J. C.; Postma, J. P. M.; van Gunsteren, W. F.; DiNola, A.; Haak, J. R. *J. Chem. Phys.* **1984**, *81*, 3684−3690.
(36) Eichinger, M.; Grubmüller, H.; Heller, H.; Tavan, P. *J. Comput. Chem.* **1997**, *18*, 1729−1749.
(37) Guillot, B. *J. Chem. Phys.* **1991**, *95*, 1543−1551.
(38) Press: W. H.; Flannery, B. P.; Teukolsky, S. A.; Vetterling, W. T. *Numerical Recipes*; Cambridge University Press: Cambridge, 1988.
(39) Brünger, A. T. Crystallographic refinement by simulated annealing. In *Crystallographic Computing 4*: *Techniques and New Technologies*; Isaacs, N. W., Taylor, M. R., Eds.; Clarendon Press: Oxford, 1988.
(40) Boys, S. F.; Bernardi, F. *Mol. Phys.* **1970**, *19*, 553.
(41) Becker, E.; Charney, E.; Anno, T. *J. Chem. Phys.* **1965**, *42*, 942.
(42) Zhao, X.; Imahori, H.; Zhan, C.-G.; Mizutani, Y.; Sakata, Y.; Kitagawa, T. *Chem. Phys. Lett.* **1996**, *262*, 643−648.
(43) Nyquist, R. A.; Luoma, D. A.; Putzig, C. L. *Vib. Spectrosc.* **1992**, *3*, 181−210.
(44) Raymond, K. S.; Grafton, A. K.; Wheeler, R. A. *J. Phys. Chem. B* **1997**, *101*, 623−631.
(45) To exclude other algorithmic causes, we have carefully checked by visual inspection that the MD trajectory of the dipole moment $M(t)$ is everywhere smooth and bears no signatures of algorithmic noise, which might arise from the multiple time-step procedures[46] applied for the integration of the Newtonian equations or from the multiple scale approach[36,11] used for the computation of the electrostatics (see Eichinger[8,47] for a discussion of accuracy issues in DFT/MM-MD simulations).
(46) Grubmüller, H.; Tavan, P. *J. Comput. Chem.* **1998**, *19*, 1534−1552.
(47) Eichinger, M. *Berechnung molekularer Eigenschaften in komplexer Lösungsmittelumgebung*: *Dichtefunktionaltheorie kombiniert mit einem Molekularmechanik-Kraftfeld*, Thesis, Ludwig-Maximilians Universität München, Germany, 1999.